

# Hybrid equation of state with pasta phases and third family of compact stars I: Pasta phases and effective mixed phase model

K. Maslov,<sup>1,2,\*</sup> N. Yasutake,<sup>3,†</sup> A. Ayriyan,<sup>4,‡</sup> D. Blaschke,<sup>5,2,1,§</sup> H. Grigorian,<sup>4,¶</sup> T. Maruyama,<sup>6</sup> T. Tatsumi,<sup>7</sup> and D. N. Voskresensky<sup>1,2,\*\*</sup>

<sup>1</sup>*National Research Nuclear University (MEPhI), Kashirskoe Shosse 31, 115409 Moscow, Russia*

<sup>2</sup>*Bogoliubov Laboratory for Theoretical Physics, Joint Institute for Nuclear Research, Joliot-Curie street 6, 141980 Dubna, Russia*

<sup>3</sup>*Department of Physics, Chiba Institute of Technology (CIT), 2-1-1 Shibazono, Narashino, Chiba, 275-0023, Japan*

<sup>4</sup>*Laboratory for Information Technologies, Joint Institute for Nuclear Research, Joliot-Curie street 6, 141980 Dubna, Russia*

<sup>5</sup>*Institute of Theoretical Physics, University of Wrocław, Max Born place 9, 50-204 Wrocław, Poland*

<sup>6</sup>*Advanced Science Research Center, Japan Atomic Energy Agency, Tokai, Ibaraki 319-1195, Japan*

<sup>7</sup>*Department of Physics, Kyoto University, Kyoto 606-8502, Japan*

(Dated: June 20, 2022)

We investigate the effect of the pasta phases formation on the quark-hadron phase transition for a set of relativistic mean-field equations of state for both hadron and quark matter. The results are compared with a mimicking construction, which was used in a recent study of the robustness of the third family solution instead of the full numerical solution with pasta phases. We demonstrate, that the construction allows for describing the numerical results well and obtain a one-to-one map of the parameter of the construction to the physical surface tension. For each pair of the models we determined the critical value of the surface tension, above which the phase transition becomes close to the Maxwell construction. It agrees qualitatively with earlier theoretical estimates.

PACS numbers: 26.60-c, 97.60.Jd, 21.65.-f, 12.39.-x

## I. INTRODUCTION

The recent discovery of pulsars with precisely measured masses close to  $2 M_{\odot}$  such as PSR J0348+432 [1] provided a new observational constraint on the equation of state (EoS) of cold dense matter under compact star (CS) conditions of  $\beta$ -equilibrium and global charge neutrality. It allowed to exclude many models of CS matter for which the EoS is too soft to describe pulsars with a mass as high as  $2 M_{\odot}$ . A new quality in the quest for the high-density EoS will be achieved when the NICER experiment [2] on board of the International Space Station will provide an accurate radius measurement with a 0.5 km uncertainty scale of the nearest millisecond pulsar PSR J0437-4715 with a known mass of  $1.44 \pm 0.07 M_{\odot}$  [3].

In this context it is interesting to study various possible phase transitions in the strongly interacting CS medium. One of them is the transition from the hadronic to the deconfined quark matter phase. Its possible description and effects on the CS mass-radius diagram were studied by many authors, see [5] and references therein. One of the potentially observable phenomena is the existence of a third CS branch in the CS mass-radius diagram,

disconnected from that of neutron stars (NSs). Such a third family branch can form if there is a strong first-order phase transition [6], e.g., from hadrons to quarks with a sufficiently large jump in the energy density taking place inside the CS [7]. A robust observation of pulsars with similar masses and substantially different radii (CS twin configurations) would reveal the existence of the first-order phase transition at zero temperature and thus prove the existence of the QCD critical endpoint [8].

One of the features of the first order hadron-quark phase transition is the appearance of the finite-size structures. They can appear in the CS matter due to existence of two separately conserved charges – baryon number and electric charge, which have to be equal in both phases to satisfy the Gibbs conditions for the phase equilibrium. The electric charge has to be globally equal to zero for gravitationally self-bound objects like NSs. Ref. [9] suggested the presence of a wide region of mixed phase at any first order phase transition in multi-component systems of charged particles, cf. further discussion of this subject in [10]. If the global electric neutrality and the existence of the surface tension between hadron and quark matter are taken into account, then the ground state of the mixed phase consists of the finite-size droplets of one phase inside another of various geometries and sizes. As has been demonstrated in [11], for the appearance of the structured mixed hadron-quark phase the Coulomb plus surface energy per droplet of the new phase should have a minimum, as a function of the droplet size. Charge screening effects were disregarded. However, as was shown in [12, 13], taking into account of the charge rearrangement due to the charge screening in

\*Electronic address: maslov@theor.mephi.ru

†Electronic address: nobutoshi.yasutake@p.chibakoudai.jp

‡Electronic address: ayriyan@jinr.ru

§Electronic address: blaschke@ift.uni.wroc.pl

¶Electronic address: hovikgrigorian@gmail.com

\*\*Electronic address: d.voskresensky@gsi.de

the pasta phases, has a large effect on the mixed hadron-quark phase. In particular, for a given pair of hadron and quark EoS there exists such a critical value of the surface tension parameter  $\sigma_c$ , governed by the charge screening effects, that for any  $\sigma > \sigma_c$  the resulting mixed phase will be given by the Maxwell construction (MC) case. Ref. [14] argued for importance of taking into account finite size effects at hadron-quark transition in heavy hybrid stars, with mass as high as  $M \gtrsim 2M_\odot$ .

The presence of the mixed phase in the phase transition region results in blurring of the energy jump, which is required for existence of the third family. Also it leads to a deviation increase of the pressure  $P(\mu)$  from the constant value  $P_c$  on the MC, which can be characterized by a relative pressure excess  $\Delta_P = \Delta P(\mu = \mu_c)/P_c$ , where  $\mu_c$  is the chemical potential, corresponding to the MC. In order to estimate the impact of the mixed phase existence on the high-mass twin (HMT) phenomenon, in [15] a phenomenological approach was used to mimic the deviation of the pressure from the MC due to the structure formation. It was found that the existence of HMTs is spoiled, if the pasta phase gives leads to  $\Delta_P > 0.05$ .

The purpose of this work is to investigate the correspondence between the phenomenological construction used before and the properties of an actual pasta calculation. In order to do this, we compute numerically the EoS of the hybrid star matter with pasta structures included for a set of surface tension values  $\sigma$  and then find a correspondence between  $\sigma$  and  $\Delta_P$ . As an input we use recently developed relativistic mean-field (RMF) EoSs for hadron [16] and quark matter [17], labeled as KVORcut and SFM, respectively. Each of them contains a free parameter, allowing to change their stiffness and thus control the features of the mass-radius (MR) diagram. We choose 2 hadronic and 2 quark parameterizations, such as all the pairs of hybrid EoSs contain the twin NS configurations and simultaneously pass the  $2M_\odot$  constraint for the maximum CS mass. After obtaining the  $\Delta_P(\sigma)$  for all the combinations of the models, we compare it with the analytical expression, investigate its model dependence and the maximum possible impact on the CS properties.

## II. HYBRID EQUATION OF STATE WITH PASTA PHASES

In this section, we outline the description of a quark-hadron hybrid EoS with structures in the mixed phase (so-called "pasta phases") following Ref. [14] and describe the recently proposed effective mixed phase construction [15, 24] with the parameter  $\Delta_P(\sigma)$  that may in turn be related to the value of the surface tension  $\sigma$ . The input to the pasta phase calculations is the energy per particle in the hadron (H) and quark (Q) matter phases, respectively. Both these functions are parameterized as

$$E^{(H,Q)}(n_B, \beta) = E_{\text{sym}}^{(H,Q)}(n_B) + \beta_{(H,Q)}^2 E_{\text{asym}}^{(H,Q)}(n_B), \quad (1)$$

where  $E_{\text{sym}}^{(H,Q)}$  and  $E_{\text{asym}}^{(H,Q)}$  are the energies per particle in symmetric matter and the asymmetry energy, respectively, in the hadron (H) and quark (Q) matter phases, and the asymmetry parameters for hadron and quark matter are defined as

$$\beta_{(H)} = 1 - 2 \frac{n_p}{n_B},$$

$$\beta_{(Q)} = \frac{n_d - n_u}{n_d + n_u} = \frac{n_d - n_u}{3n_B}.$$

As the microscopical input to the pasta phases code, we provide polynomial fit formulas for these EoS.

### A. Hadronic phase

The description of the hadronic matter phase is based on a RMF model with hadron masses and couplings dependent on the scalar field  $\sigma$  developed in [16, 18]. Within this approach all the hadron effective masses decrease in the medium with the same rate as functions of the mean  $\sigma$  field, in accordance with the idea of the partial chiral symmetry restoration. Phenomenological scaling functions enter the EoS only in combinations

$$\eta_M(\sigma) = \frac{\Phi_M^2(\sigma)}{\chi_M^2(\sigma)}, \quad (2)$$

where the subscript  $M = \sigma, \omega, \rho, \phi$  labels the meson fields included into the model. In this framework the KVORcut family of the models was constructed, which allows for a high maximum CS mass and simultaneously fulfills a majority of other constraints. We focus here on the KVORcut02 and KVORcut03 models, in which the additional stiffness is introduced as outlined in [19] to allow for the description of pulsars with a mass of  $\sim 2M_\odot$  [1] even when hyperons and  $\Delta$ -resonances are present in the EoS. The KVORcut02 model is the stiffest one, while the softer KVORcut03 model passes constraints for the pressure as a function of the baryon density following from analyses of flows in heavy-ion collisions [20, 21].

The hadronic EoS can be parametrized with

$$E_{\text{sym}}^{(H)}(n_B) = \sum_{i=0}^{20} a_i u^i, \quad E_{\text{asym}}^{(H)}(n_B) = \sum_{i=0}^{20} b_i u^i, \quad (3)$$

where  $u = n_B/n_0$  is the nuclear compression with  $n_0 = 0.16 \text{ fm}^{-3}$  being the nuclear saturation density. The coefficients  $a_i, b_i$  are the fit parameters given in Table I.

### B. Quark matter phase

For description of the quark phase we use the recently developed RMF density functional [17], inspired by the string-flip model [22, 23]. This approach gives a simple way to model the confinement of quarks via introducing divergent quark masses for low baryon densities and the

TABLE I: Parameters of the hadronic EoS fits given by Eq. (3), in units of MeV.

	$a_0$	$a_1$	$a_2$	$a_3$	$a_4$	$a_5$	$a_6$	$a_7$	$a_8$	$a_9$	$a_{10} \cdot 10^3$
KVORcut02	0.81351	-34.683	33.997	-56.44	72.585	-47.173	18.49	-4.7982	0.8607	-0.10787	9.2105
KVORcut03	1.3516	-36.250	19.305	7.0831	-16.110	13.457	-6.3007	1.8621	-0.36858	0.049935	-4.5546
		$a_{11} \cdot 10^4$	$a_{12} \cdot 10^6$	$a_{13} \cdot 10^7$	$a_{14} \cdot 10^8$	$a_{15} \cdot 10^{10}$	$a_{16} \cdot 10^{11}$	$a_{17} \cdot 10^{12}$	$a_{18} \cdot 10^{13}$	$a_{19} \cdot 10^{15}$	$a_{20} \cdot 10^{17}$
KVORcut02		-4.8153	8.2274	7.5668	-5.4597	3.6447	12.955	-8.1609	2.4357	-3.8209	2.5408
KVORcut03		2.5440	-5.0889	-3.7728	3.0135	-2.8021	-6.9601	4.5957	-1.4064	2.2473	-1.5170
	$b_0$	$b_1$	$b_2$	$b_3$	$b_4$	$b_5$	$b_6$	$b_7$	$b_8$	$b_9 \cdot 10^3$	$b_{10} \cdot 10^4$
KVORcut02	0.48339	47.238	-29.873	21.027	-8.8474	2.1619	-0.23286	-0.027407	0.014986	-2.7789	2.9860
KVORcut03	0.75228	43.283	-17.843	8.7129	-4.8032	2.8450	-1.2560	0.37458	-0.076074	10.623	-10.016
		$b_{11} \cdot 10^5$	$b_{12} \cdot 10^6$	$b_{13} \cdot 10^8$	$b_{14} \cdot 10^9$	$b_{15} \cdot 10^{11}$	$b_{16} \cdot 10^{11}$	$b_{17} \cdot 10^{12}$	$b_{18} \cdot 10^{14}$	$b_{19} \cdot 10^{16}$	$b_{20} \cdot 10^{18}$
KVORcut02		-1.8742	0.45587	2.5343	-2.3493	2.9652	0.52260	-0.36619	1.1538	-1.8825	1.2923
KVORcut03		5.8272	-1.2946	-8.1827	7.1581	-8.4830	-1.6147	1.1263	-3.5671	5.8735	-4.0798

TABLE II: Parameters of the quark SFM EoS fits given by Eq. 4. All units are MeV except for  $\gamma_{a,s}$  which are dimensionless.

	$\alpha_s$	$\beta_s$	$\gamma_s$	$\delta$	$\alpha_a$	$\beta_a$	$\gamma_a$
$\alpha = 0.2$	-1.7641	1.6654	0.33419	0.98796	-0.02570	0.052563	0.0085143
$\alpha = 0.3$	-6.8814	3.3411	4.5326	0.21680	-0.029531	0.056170	0.018573

density-dependent screening effect. The effective screening is described analogously to the excluded volume effect in models of hadronic matter with density-dependent couplings.

Together with these features, the model incorporates a repulsive vector interaction with a higher-order density dependence. It gives a relatively soft EoS near the phase transition point, which becomes much stiffer as the density increases. This stiffness allows for description of the  $2M_\odot$  CS mass constraint for hybrid stars. However, the soft behavior near the phase transition (PT) leads to the possibility of HMT CS configurations, which appear for a large enough density jump for the appearance of a separate branch of hybrid stars dubbed as a "third family" of CSs. Further details on these models can be found in [17].

This EoS can be parametrized using

$$\begin{aligned} E_{\text{sym}}^{(Q)}(n_B) &= \alpha_s + \beta_s u^{-1/3} + \gamma_s u^{1/3} + \delta u, \\ E_{\text{asym}}^{(Q)}(n_B) &= \frac{\alpha_a u}{1 + \gamma_a u^2} + \beta_a u^{2/3}, \end{aligned} \quad (4)$$

where  $\alpha_{a,s}, \beta_{a,s}, \gamma_{a,s}$  and  $\delta$  are the fit parameters given in Table II.

### C. Pasta phase calculation

In order to study the finite-size structures, we require the Gibbs conditions

$$P^{(H)} = P^{(Q)}, \quad \mu_B^{(H)} = \mu_B^{(Q)}, \quad \mu_e^{(H)} = \mu_e^{(Q)} \quad (5)$$

to be fulfilled within the mixed phase region. In the Wigner-Seitz (WS) approximation the space is considered as tessellated by cells of a given geometry depending on the dimensionality  $d$ : spheres for  $d = 3$ , cylinders for

$d = 2$ , and slabs for  $d = 1$  with a volume  $V_W$ . Within each of the cells the quark phase of the volume  $V_Q$  is embedded into the surrounding hadron phase of the volume  $V_H$  or vice versa. If the hadron phase is dominant the structures are dubbed "droplets" and "rods" for  $d = 3$  and  $d = 2$ , respectively, and "bubbles" or "tubes", otherwise. The boundary layer is assumed to be smaller than any of the characteristic lengths of the problem, and thus the surface effects are captured by introducing the surface tension parameter  $\sigma$ . The value of  $\sigma$  is highly model-dependent and uncertain. In this work we vary  $\sigma$  in a wide range with a small step, which allows us to determine numerically the critical surface tension  $\sigma_c$  for all pairs of hadron and quark model under consideration.

In the Thomas-Fermi approximation the Helmholtz free energy of a cell reads:

$$\begin{aligned} \epsilon &= \int_{V_H} d^3r \mathcal{E}^{(H)}[\{n_h(r)\}] + \int_{V_Q} d^3r \mathcal{E}^{(Q)}[\{n_q(r)\}] + \epsilon_e \\ &+ \epsilon_C + \epsilon_S, \end{aligned} \quad (6)$$

where  $h = n, p$  and  $q = u, d$ ,  $\mathcal{E}^{(H)} = n_B(E^{(H)} + m_N)$  and  $\mathcal{E}^{(Q)} = n_B E^{(Q)}$  are the free energy densities of hadron and quark matter, respectively, and  $\epsilon_e, \epsilon_C, \epsilon_S$  stand for the contribution to the energy per cell from free electron gas, Coulomb effects and the surface term, respectively. The nucleon mass is  $m_N = 938$  MeV. For simplicity, in the current work we neglect the contribution of the muons. The Coulomb contribution to the energy per cell is given by

$$\epsilon_C = \frac{e^2}{2} \int_{V_{WS}} d^3r d^3r' \frac{n_{\text{ch}}(\vec{r}) n_{\text{ch}}(\vec{r}')}{|\vec{r} - \vec{r}'|}, \quad (7)$$

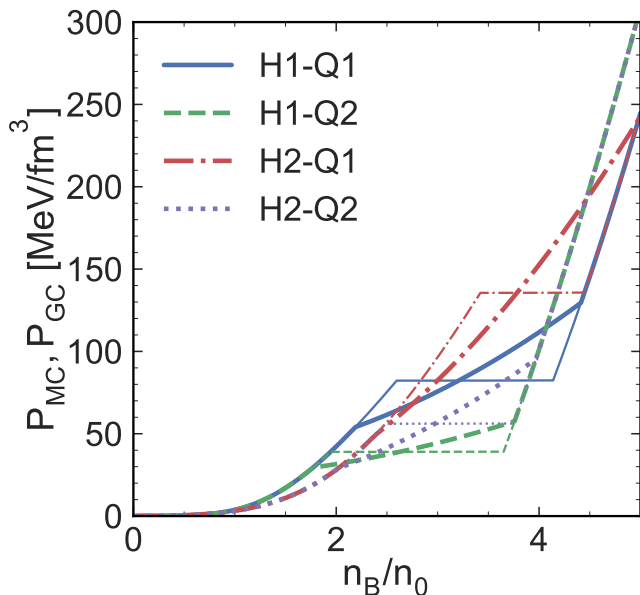


FIG. 1: Pressure as a function of the density for all the combinations of models under consideration with the MC (thin lines) and the GC with  $\sigma = 0$  and no electrostatic contribution (thick lines).

where the charge density is

$$en_{\text{ch}}(\vec{r}) = \sum_h Q_h n_h(\vec{r}) + \sum_q Q_q n_q(\vec{r}) - en_e. \quad (8)$$

Accordingly, the screened Coulomb potential  $\phi(r)$  is defined as

$$\phi(r) = - \int_{V_{WS}} d^3r' \frac{e^2 n_{\text{ch}}(\vec{r}')}{|\vec{r} - \vec{r}'|} + \phi_0, \quad (9)$$

where  $\phi_0$  is an arbitrary constant representing the gauge degree of freedom. It is fixed by the condition  $\phi(R_{WS}) = 0$ , see Ref. [14]. The selfconsistent field fulfills the Poisson equation

$$\Delta\phi(r) = 4\pi e^2 n_{\text{ch}}(r). \quad (10)$$

The equations are solved for a given baryon density

$$n_B = \frac{1}{V_{WS}} \left[ \sum_h \int_{V_H} d^3r n_h(r) + \frac{1}{3} \sum_q \int_{V_Q} d^3r n_q(r) \right] \quad (11)$$

together with the charge neutrality condition

$$\int_{V_{WS}} d^3r n_{\text{ch}}(r) = 0. \quad (12)$$

#### D. Fit formula for the phase transition

In [15] a simple modification of the MC was employed to mimic the effect of the pasta structures on the quark-hadron phase transition. If the EoSs of quark and hadron

matter are given in terms of the pressure as a function of the chemical potential  $P^{(H)}(\mu)$  and  $P^{(Q)}(\mu)$ , respectively, the pressure with this construction is given by

$$P(\mu) = \begin{cases} P^{(H)}(\mu), & \mu < \mu_{cH}, \\ a(\mu - \mu_c)^2 + b(\mu - \mu_c) \\ + P_c + \Delta P, & \mu_{cH} < \mu < \mu_{cQ}, \\ P^{(Q)}(\mu), & \mu_{cQ} < \mu, \end{cases}$$

where  $P_c = P^{(H)}(\mu_c) = P^{(Q)}(\mu_c)$ ,  $\mu_c$  is the intersection point corresponding to the MC. From this expression the baryon density can be calculated as  $n_B(\mu) = dP/d\mu$ . The four parameters  $a$ ,  $b$ ,  $\mu_{cH}$ ,  $\mu_{cQ}$  can be determined from the conditions of continuity of pressure and baryon number density  $n_B(\mu)$  at both  $\mu = \mu_{cH}$  and  $\mu = \mu_{cQ}$ , so there is only one free parameter  $\Delta P$  left.

### III. NUMERICAL RESULTS

In this section we show the results of the fits for every combination of the models. Below we use the "H-Q" notation for the pairs of the hadronic and quark models, where H = H1, H2 corresponds to KVORcut[02, 03] models, respectively, and Q = Q1, Q2 denotes the SFM model with  $\alpha = 0.2, 0.3$ , respectively.

For each pair of the models Fig. 1 demonstrates two limiting cases of the MC and the Gibbs conditions (GC) with  $\sigma = 0$  and no electrostatic contribution. For a given quark EoS the transition density and pressure is lower for a stiffer hadronic EoS H1, and for a given hadronic EoS the transition happens earlier for the softest quark EoS Q2. Thus the onset of the phase transition proves to be the lowest for the H1-Q2 case, because in this case the hadronic EoS is the stiffest one and the quark EoS is the softest in the low density region. After taking into account of the continuity of the electron chemical potential the pressure becomes non-constant within the mixed phase region. It can be seen from Fig. 1 that the pressure difference on the GC increases with an increase of the  $P_c$  of the MC. This broadening is to be compared with the critical PT broadening from [15] in order to understand whether the third branch phenomenon can be in principle eliminated by the pasta phases formation.

#### A. Comparison with phenomenological description

Possible applications of the construction (IID) require to know the limits on the realistic values of the parameters. The parameter  $\Delta P$  is greater than zero by definition and limited from above, with the maximum possible  $\Delta P$  corresponding to the zero surface tension. The exact correspondence of  $\Delta P$  to the surface tension  $\sigma$  is presented in this section.

We performed the least-squares fit of the  $P(n_B)$  derived from Eq. (IID) to describe the numerical data, us-

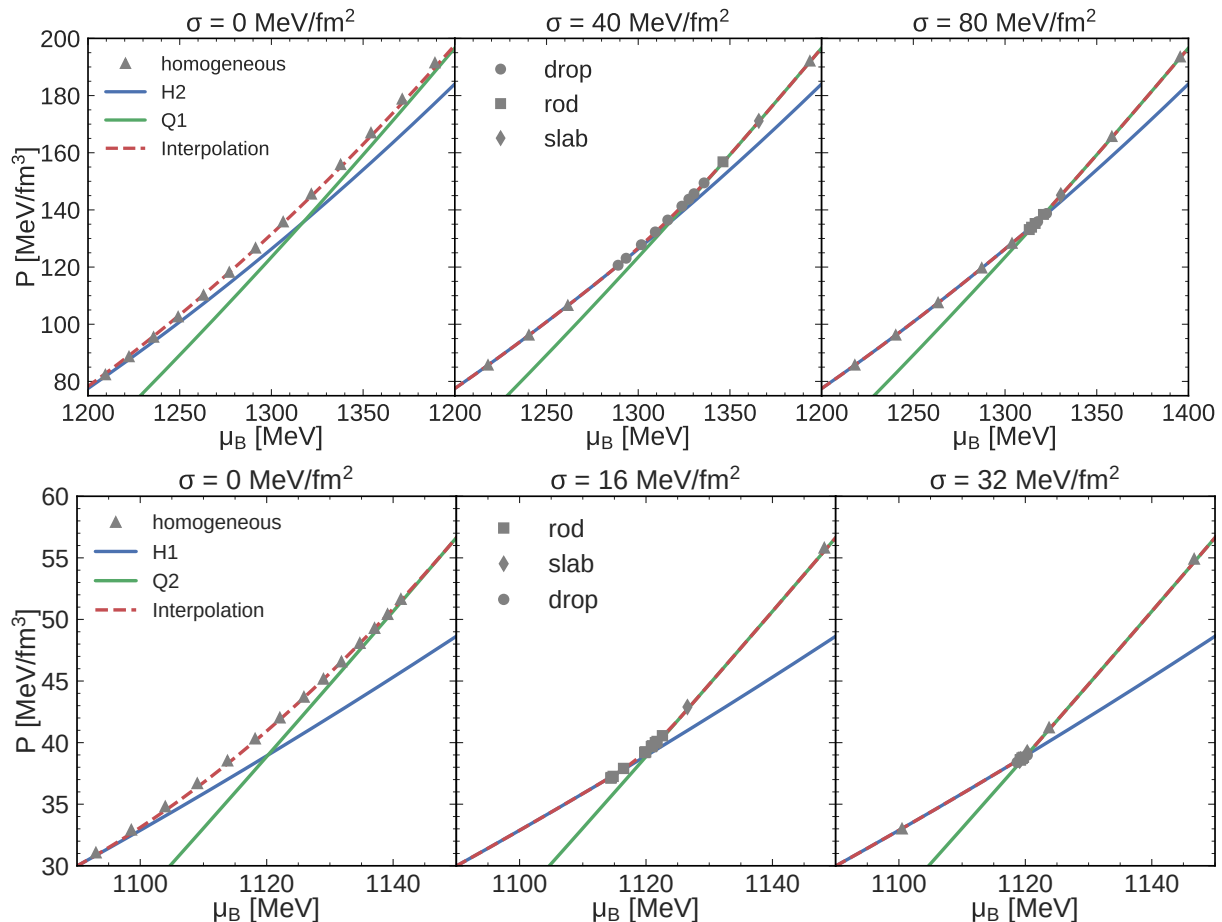


FIG. 2: Pressure as a function of the chemical potential for the H2-Q1 model for the surface tension  $\sigma = [0, 40, 80]$  MeV/fm<sup>2</sup> (upper panel) and the H1-Q2 model with  $\sigma = [0, 16, 32]$  MeV/fm<sup>2</sup> (lower panel). Solid lines denote the quark and hadron EoSs, symbols denote the numerical results with structure types indicated in the legend and the dashed lines show the best-fit curves using Eq. IID.

TABLE III: Critical pressure  $P_c$ , energy density  $\mathcal{E}_c$  and energy density jump  $\Delta\mathcal{E}$  in units of MeV/fm<sup>3</sup>, together with the best fit parameters of Eq. 15 and the theoretical estimates for all the combinations of models. Numerical critical surface tensions  $\sigma_c$  and the analytic results  $\tilde{\sigma}_c$  from Eq. (18) are given in units of MeV/fm<sup>2</sup>. The Debye lengths  $\lambda_D^{(Q),(H)}$  are given in units of fm.

Pair	$\Delta_P^{(0)}$	$\sigma_c$	$\alpha$	$\beta$	$P_c$	$\Delta\mathcal{E}$	$\mathcal{E}_c$	$\tilde{\sigma}_c$	$\tilde{\beta}$	$\lambda_D^{(Q)}$	$\lambda_D^{(H)}$
H1-Q1	0.052	55.2	1.13	0.68	82	121	617	59.1	0.50	3.79	5.87
H1-Q2	0.052	31.4	1.12	0.62	39	103	512	30.5	0.25	3.96	6.40
H2-Q1	0.047	72.7	1.06	0.86	135	109	682	87.5	0.74	3.71	5.44
H2-Q2	0.060	36.6	0.83	0.61	56	87	546	46.3	0.38	3.93	5.99

ing  $\Delta P$  as a variational parameter. Fig. 3 shows examples of the fitting results for the H2-Q1 combination of models for the surface tension values  $\sigma = [0, 40, 80]$  MeV/fm<sup>2</sup>. Dots show the numerical results for the pasta structures, solid lines denote the initial hadron and quark EoSs and the best fit by formula Eq. IID is shown by

the dashed line. We see that the phenomenological construction we employed in previous works can adequately describe the exact numerical result. The quality of the fit can be characterized by the root-mean-square deviation, defined as

$$\chi = \sqrt{\frac{1}{N} \sum_{i=1}^N \left( \frac{P_{\text{fit}}(n_B^{(i)}) - P_i}{P_i} \right)^2}, \quad (13)$$

where  $P_i$  and  $n_B^{(i)}$  are the calculated numeric data points,  $P_{\text{fit}}(n_B)$  is given by Eq. (IID), and  $N$  is the number of the data points in the range of densities, where the pasta structures exist. For the cases shown in the upper panel of Fig. 3 the r.m.s. deviation  $\chi$  equals to 3.5%, 1.0%, 1.6% for  $\sigma = [0, 40, 80]$  MeV/fm<sup>2</sup>, respectively. With such a precision the use of the interpolating construction, given by Eq. (IID), for mimicking the pasta phase effects on the EoS is justified.

Similar fits were performed for a set of surface tension values in the range (0 – 80) MeV/fm<sup>2</sup>. In Fig. 4 we demonstrate thus obtained curves  $\Delta_P(\sigma)$  for all the com-

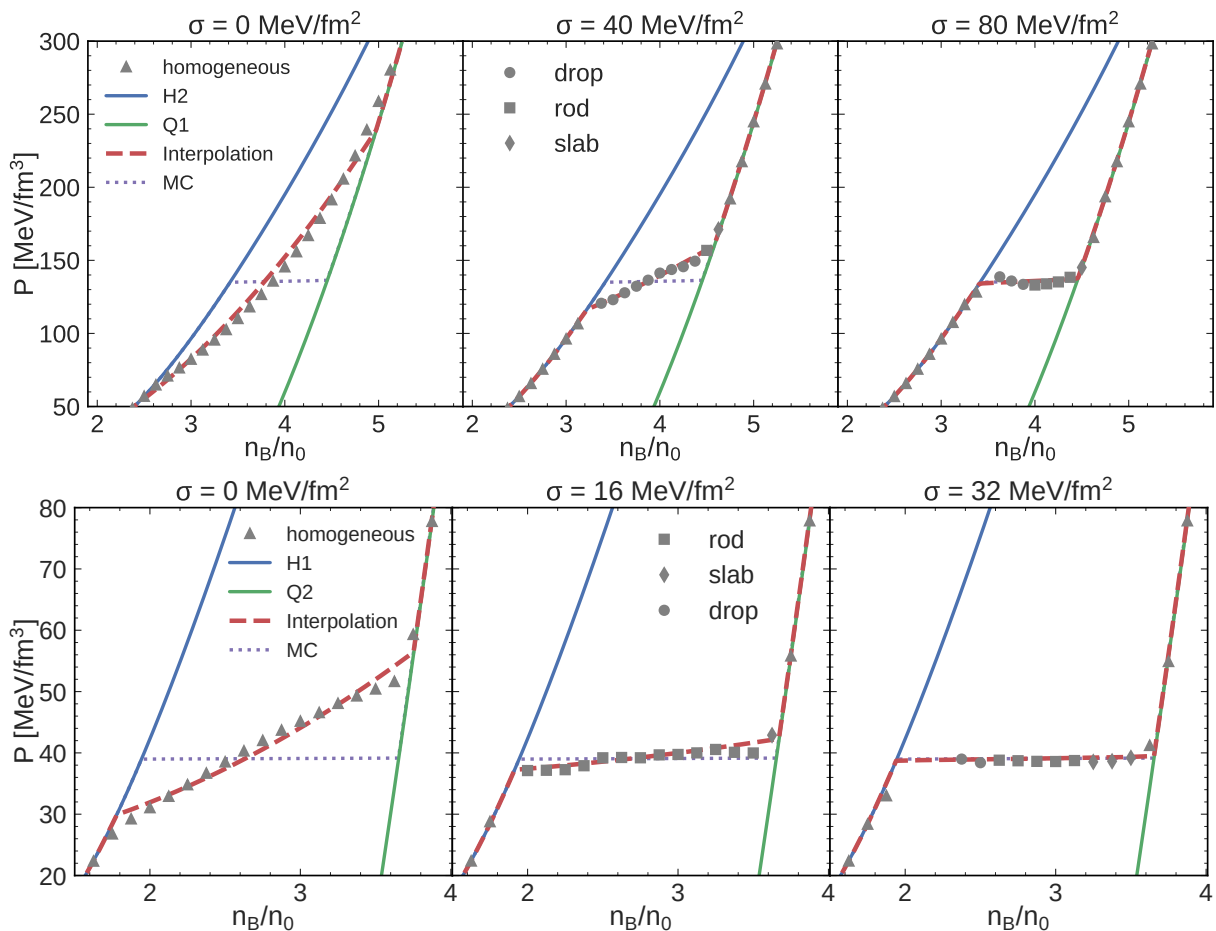


FIG. 3: Pressure as a function of the baryon density for the H2-Q1 model for the surface tension  $\sigma = [0, 40, 80]$  MeV/fm<sup>2</sup> (upper panel) and the H1-Q2 model with  $\sigma = [0, 16, 32]$  MeV/fm<sup>2</sup> (lower panel). Solid lines denote the quark and hadron homogeneous matter EoSs, symbols denote the numerical results with the structure type indicated in the legend and the dashed lines show the best-fit curves using Eq. IID. For comparison, we show also the MC by a dotted line.

combination of the models by solid lines. It is clearly seen that if the surface tension exceeds some critical value  $\sigma_c$ , the effect of the finite-size structures becomes negligible. However, the pressure excess  $\Delta_P$  does not become exactly zero, since in the MC case the WS cell size would become infinite, but the numeric code has a large but finite limiting cell size. Thus the code we used is applicable only for  $\sigma < \sigma_c$ . Nevertheless, the resulting pressure in the  $\sigma > \sigma_c$  is very close to the MC line, and is best-fitted by a very low  $\Delta_P$ .

### B. Model dependence of the critical surface tension

Because of non-exact reproducing of the MC line in the case of large surface tension  $\sigma$ , we need to perform an additional step to define the critical surface tension  $\sigma_c$  in a reproducible manner. For this we used a fit of the

$\Delta_P(\sigma)$  curve with the following ansatz

$$\Delta_P(\sigma) = \Delta_P^{(0)} S\left(\frac{\sigma}{\sigma_c}; \alpha, \beta\right), \quad (14)$$

$$S(x; \alpha, \beta) = e^{-x} (1 - x^\beta)^\alpha \theta(1 - x), \quad (15)$$

where  $\Delta_P^{(0)}$ ,  $\alpha$ ,  $\beta$  and  $\sigma_c$  are the parameters of the fit, and  $\theta(x)$  is the step function. The parameter values thus determined are summarized in Table III. The solid lines in the upper panel of Fig. 4 show the best fit curves given by Eq. (15).

The dimensionless function  $S(x)$  shown in the lower panel of Fig. 4 is only weakly model dependent. By the solid line with dots we show the function  $S(x; \bar{\alpha}, \bar{\beta})$ , where

$$\bar{\alpha} = 1.037, \quad \bar{\beta} = 0.692 \quad (16)$$

are the mean values of the parameters. The confidence region of  $S(x)$  according to their standard deviations  $\Delta\bar{\alpha} = 0.121$  and  $\Delta\bar{\beta} = 0.098$  is shown by the shaded area. The same shaded area is plotted as a function of the

dimensionful  $\sigma$  in the upper panel for the H1-Q1 model as an example, with the best-fit  $\Delta_P^{(0)}$ .

In order to describe the model dependence of the critical surface tension  $\sigma_c$  we choose the pressure on the MC line  $P_c$  as the parameter characterizing a pair of models. We show the dependence of  $\sigma_c$  on  $P_c$  in Fig. 5 by solid symbols. It is clear that within the current set of models the critical surface tension monotonously grows with an increase of the pressure  $P_c$ . It is interesting to compare this dependence with the expression for  $\sigma_c$  obtained in [13] obtained analytically using the linearized Poisson equation. The resulting expression involves the Debye screening lengths and the values of the electric field in the both phases. At the critical chemical potential  $\mu_B = \mu_{c,B}^{(H)}$  of the phase transition we have  $\mu_{e,\text{Gibbs}} = \mu_{e,\text{bulk}}^{(H)}$ . When the quark matter fraction is small, the size of the hadron phase is much larger than the screening length. Thus we can consider it to be electrically neutral with  $\mu_e = \mu_{e,\text{bulk}}^{(H)}$ . The electron contribution to the quark matter charge can be neglected [13]. Hence all the values are to be evaluated at  $\mu_B = \mu_{c,B}^{(H)}$ , and  $\mu_e = \mu_{e,\text{bulk}}^{(H)}$  for hadronic matter and  $\mu_e = 0$  for quark matter. The Debye screening lengths are evaluated as

$$\left(\frac{1}{\lambda_D^{(H,Q)}}\right)^2 = -4\pi e^2 \left(\frac{\partial n_{\text{ch}}^{(H,Q)}}{\partial \mu_e}\right)_{\mu_B} \quad (17)$$

where  $e^2 = 1/137$  and  $n_{\text{ch}}^{(H,Q)}(\mu_B, \mu_e)$  is the charge density of the phase  $H$  or  $Q$ . They can be expressed through Landau parameters of beta-equilibrium matter, though in this work we calculated the derivatives numerically. The expression for the critical surface tension is (see Eq. (77) of Ref. [13])

$$\tilde{\sigma}_c = \lambda_D^{(Q)} \frac{\tilde{\alpha}\tilde{\beta}(\tilde{\alpha} + 4/3)}{3(1 + \tilde{\alpha})^2}, \quad \tilde{\alpha} = \frac{\lambda_D^{(Q)}}{\lambda_D^{(H)}}, \quad \tilde{\beta} = \frac{3(U_0^{\text{II}} - U_0^{\text{I}})^2}{8\pi e^2 (\lambda_D^{(Q)})^2}, \quad (18)$$

where the parameters of the electric field contribution are  $U_0^{\text{II}} \simeq -\mu_{e,\text{bulk}}^{(H)}$  and  $U_0^{\text{I}} = -4\pi e^2 (\lambda_D^{(Q)})^2 n_{\text{ch}}^{(Q)}(\mu_B = \mu_c, \mu_e = 0)$ .

Thus obtained values of the parameters and  $\tilde{\sigma}_c$  are summarized in the Table III. In the Fig. 5 the values of  $\tilde{\sigma}_c$  are plotted against the pressure on the MC line  $P_c$  by the empty symbols. We see that thus evaluated theoretical values are consistent with the numerical result. Thus we confirm that the numerical calculation correctly captures the essential physics of the pasta phase formation and prove the usability of the linearized Poisson equation for the description of the electric field.

#### IV. CONCLUSION

In this work we investigated the modification of quark-hadron hybrid equations of state due to the formation of

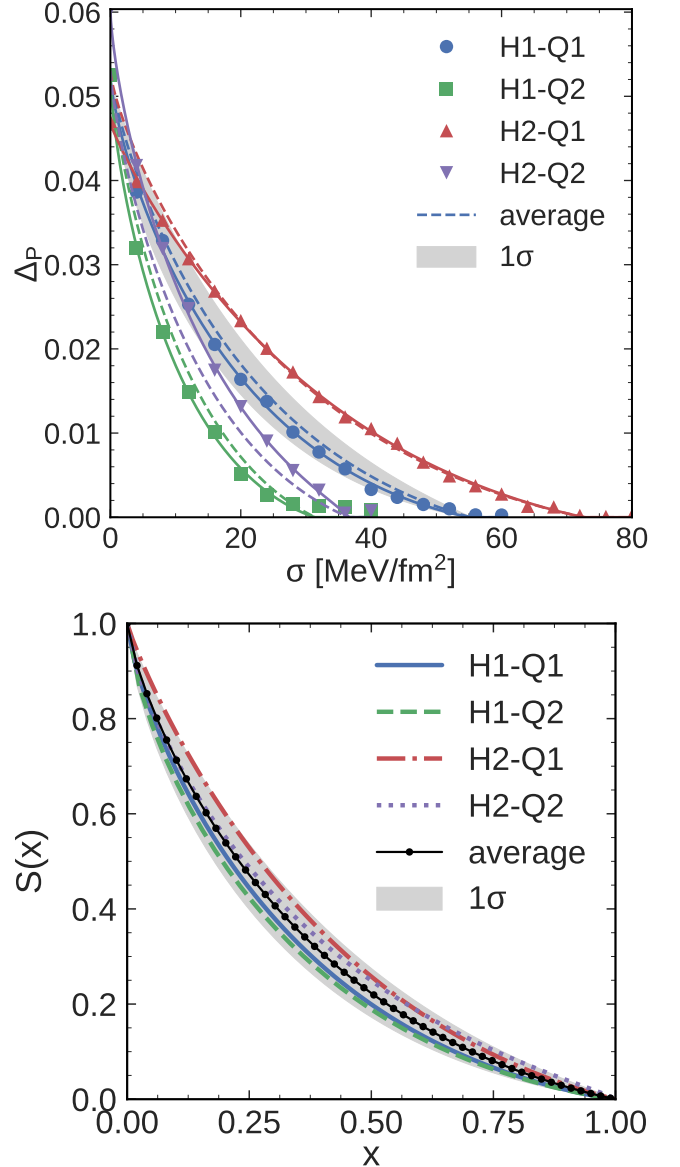


FIG. 4: Upper panel: Relative pressure shift  $\Delta_P$  at the MC chemical potential  $\mu_c$  as a function of the surface tension  $\sigma$  for all the combinations of models. Solid lines show the results of the fit with use of Eq. (15), and the dashed lines are plotted with use of the mean values of  $\alpha$  and  $\beta$  from (16) and the best-fit  $\Delta_P^{(0)}$  and  $\sigma_c$  for each model. Lower panel: The dimensionless function  $S(x)$  (15) for our models. The solid line with dots shows  $S(x)$  for the mean values of  $\alpha$  and  $\beta$ , and the shaded area indicates the change of  $S(x)$  for the  $1\sigma$  range of  $\alpha$  and  $\beta$ .

structures (pasta phases) in the mixed phase. We performed a numerical study of the pasta structures for a set of modern relativistic mean-field equations of state of quark and hadron matter. The surface tension between quark and hadron matter was treated as a free parameter and varied its value in the range  $0 - 80 \text{ MeV}$ . We have demonstrated that for all values of  $\sigma$  the numerical results



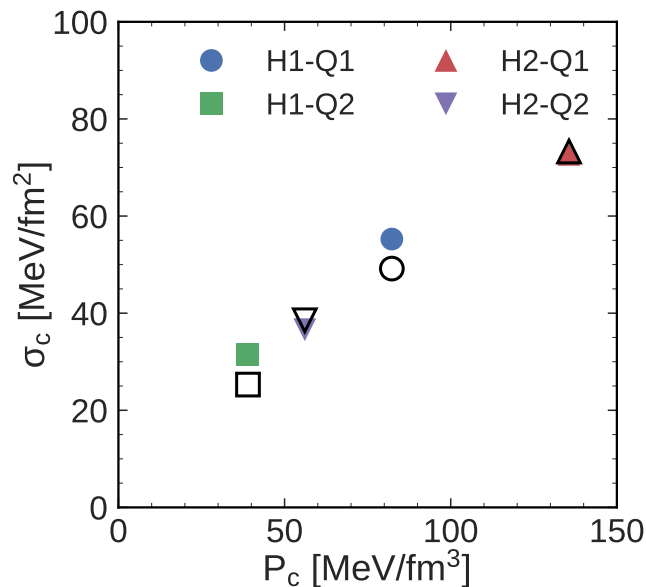


FIG. 5: Critical surface tension  $\sigma_c$  as a function of the pressure on the MC line  $P_c$  for all the combination of models considered. Full symbols denote the results of the numerical calculation, and open symbols are the analytical estimates using Eq. (18).

for the pressure in the mixed phase can be described reasonably well by a simple polynomial interpolation, which was recently introduced to study the robustness of the occurrence of a third family branch of compact stars against the formation of pasta phases. This finding justifies the application of such a construction to compact stars [15].

The parameter  $\Delta_P$  of the construction has the meaning of an additional pressure contribution relative to that at the chemical potential of the Maxwell construction. It has its origin in the finite size of the structures in

the pasta phases. As a result of the fit we obtained the functional dependence of  $\Delta_P(\sigma)$ . This map exhibits the characteristic features of such a phase transition, which we examined quantitatively. The curve  $\Delta_P(\sigma)$  decreases monotonically with increasing  $\sigma$ , and its maximum value  $\Delta_P^{\sigma=0}$  does not exceed 6% for any combination of the hadronic and quark matter models considered here. In [15] the upper limit of  $\Delta_P$  for existence of a third family of compact stars was found to be of the same order. This means that in the realistic case of a non-zero  $\sigma$  the third branch of compact stars will be robust against the formation of pasta structures.

It is known that when one accounts for the electric field, there exists a critical value of the surface tension  $\sigma_c$ , such that for any  $\sigma > \sigma_c$  the formation of structures becomes energetically disfavored and the phase transition degenerates to a Maxwell construction with  $\Delta_P \simeq 0$ . We found the resulting values of  $\sigma_c$  for the models under consideration. Interestingly,  $\sigma_c$  increases monotonically with the critical pressure  $P_c$  of the Maxwell construction for a given pair of hadron and quark models. We adapted the analytical consideration of [13] to our models and showed that the analytically evaluated critical surface tension is quantitatively consistent with the numerical results. The existence of the third family requires the phase transition to happen at rather low densities. Therefore, lower values of  $P_c$  correspond to models with twin star configurations. Consequently, the critical surface tension for such models should be also lower, and a larger range of  $\sigma$  values will not spoil the existence of the third family.

**Acknowledgments.** We would like to thank David Alvarez-Castillo and Niels-Uwe Bastian for valuable discussions. This work has been supported by the Russian Science Foundation under grant No. 17-12-01427. K.M. acknowledges the hospitality of the Chiba Institute of Technology, where a part of this work was done.

- 
- [1] J. Antoniadis *et al.*, *Science* **340**, 1233232 (2013) doi:10.1126/science.1233232 [arXiv:1304.6875 [astro-ph.HE]].
- [2] <https://heasarc.gsfc.nasa.gov/docs/nicer>
- [3] D. J. Reardon *et al.*, *Mon. Not. Roy. Astron. Soc.* **455**, no. 2, 1751 (2016) doi:10.1093/mnras/stv2395 [arXiv:1510.04434 [astro-ph.HE]].
- [4] B. P. Abbott *et al.* [LIGO Scientific and Virgo Collaborations], *Phys. Rev. Lett.* **119**, no. 16, 161101 (2017) doi:10.1103/PhysRevLett.119.161101 [arXiv:1710.05832 [gr-qc]].
- [5] D. Blaschke and N. Chamel, arXiv:1803.01836 [nucl-th].
- [6] U. H. Gerlach, *Phys. Rev.* **172**, 1325 (1968). doi:10.1103/PhysRev.172.1325
- [7] S. Benic, D. Blaschke, D. E. Alvarez-Castillo, T. Fischer and S. Typel, *Astron. Astrophys.* **577**(2015) A40.
- [8] D. Blaschke, D. E. Alvarez-Castillo and S. Benic, *PoS CPOD 2013*, 063 (2013) [arXiv:1310.3803 [nucl-th]].
- [9] N. K. Glendenning, *Phys. Rev. D* **46**, 1274 (1992). doi:10.1103/PhysRevD.46.1274
- [10] N. K. Glendenning, *Compact Stars: Nuclear Physics, Particle Physics, and General Relativity*, 2nd ed., Springer-Verlag, N. Y., 2000.
- [11] H. Heiselberg, C. J. Pethick and E. F. Staubo, *Phys. Rev. Lett.* **70**, 1355 (1993). doi:10.1103/PhysRevLett.70.1355
- [12] D. N. Voskresensky, M. Yasuhira and T. Tatsumi, *Phys. Lett. B* **541**, 93 (2002) doi:10.1016/S0370-2693(02)02186-X [nucl-th/0109009].
- [13] D. N. Voskresensky, M. Yasuhira and T. Tatsumi, *Nucl. Phys. A* **723**, 291 (2003) doi:10.1016/S0375-9474(03)01313-7 [nucl-th/0208067].
- [14] N. Yasutake, R. Lastowiecki, S. Benic, D. Blaschke, T. Maruyama and T. Tatsumi, *Phys. Rev. C* **89**, 065803 (2014) doi:10.1103/PhysRevC.89.065803 [arXiv:1403.7492 [astro-ph.HE]].
- [15] A. Ayriyan, N.-U. Bastian, D. Blaschke, H. Grigorian, K. Maslov and D. N. Voskresensky, *Phys. Rev. C* **97**, no. 4, 045802 (2018) doi:10.1103/PhysRevC.97.045802



- [arXiv:1711.03926 [nucl-th]].
- [16] K. A. Maslov, E. E. Kolomeitsev and D. N. Voskresensky, Nucl. Phys. A **950** (2016) 64.
- [17] M. A. R. Kaltenborn, N. U. F. Bastian and D. B. Blaschke, Phys. Rev. D **96**, no. 5, 056024 (2017) doi:10.1103/PhysRevD.96.056024 [arXiv:1701.04400 [astro-ph.HE]].
- [18] E. E. Kolomeitsev and D. N. Voskresensky, Nucl. Phys. A **759**, 373 (2005). doi:10.1016/j.nuclphysa.2005.05.154 [nucl-th/0410063].
- [19] K. A. Maslov, E. E. Kolomeitsev and D. N. Voskresensky, Phys. Rev. C **92**, no. 5, 052801 (2015) doi:10.1103/PhysRevC.92.052801 [arXiv:1508.03771 [astro-ph.HE]].
- [20] P. Danielewicz, R. Lacey and W. G. Lynch, Science **298**, 1592 (2002) doi:10.1126/science.1078070 [nucl-th/0208016].
- [21] W. G. Lynch, M. B. Tsang, Y. Zhang, P. Danielewicz, M. Famiano, Z. Li and A. W. Steiner, Prog. Part. Nucl. Phys. **62**, 427 (2009) doi:10.1016/j.ppnp.2009.01.001 [arXiv:0901.0412 [nucl-ex]].
- [22] C. J. Horowitz, E. J. Moniz and J. W. Negele, Phys. Rev. D **31**, 1689 (1985).
- [23] G. Röpke, D. Blaschke and H. Schulz, Phys. Rev. D **34**, 3499 (1986).
- [24] A. Ayriyan and H. Grigorian, EPJ Web Conf. **173**, 03003 (2018) doi:10.1051/epjconf/201817303003 [arXiv:1710.05637 [astro-ph.HE]].